Electromagnetic transitions from isobaric analog states to study nuclear matrix elements for neutrinoless $\beta\beta$ decays and astro-neutrino inverse β decays

Hiroyasu Ejiri [*]

Research Center for Nuclear Physics, Osaka University, Osaka 567-0047, Japan

Experimental studies of nuclear matrix elements (NMEs) for neutrinoless double-β decays (DBDs) and astro-neutrino (ν) inverse β decays (IBDs) are crucial for ν studies beyond the standard model and the astro-ν studies since accurate theoretical calculations of the NMEs are hard due to the high sensitivity of the NMEs to the nuclear models and the nuclear parameters used for the models. Some of the important NMEs of electromagnetic transition operators associated with DBD and IBD, including the effective weak couplings, are found to be experimentally obtained by measuring the corresponding electromagnetic gamma (EM:γ) transitions from the isobaric analog states (IASs) of the DBD and IBD nuclei. Then the experimental NMEs and the couplings are used for evaluating the DBD and IBD NMEs and for checking the model calculations. The EM-NMEs, the cross sections, and the event rates for the IAS-γ transitions are estimated for DBD and IBD nuclei to show the feasibility of the experiments.

Introduction. Neutrinoless double-β decay (DBD $\beta\beta$) is a sensitive and realistic probe for studying the neutrino (ν) nature (Majorana or Dirac), the absolute ν-mass scale, the right-handed weak current (RHC), and others, which are beyond the standard model, as discussed in reviews [1–3]. Astro-ν productions, astro-ν syntheses, and astro-ν-oscillations are of great interest for physics of astro-neutrinos and supernovae and are studied by nuclear charged-current (CC) interaction, i.e., inverse β decay (IBD). The DBD and IBD rates are proportional to their neutrino nuclear responses, i.e., the squares of the nuclear matrix elements (NMEs). The present letter addresses the NMEs, which are indispensable for the ν studies by these rare nuclear decays.

The DBD ν-mass process involves the Majorana ν exchange between two nucleons in the DBD nucleus. Then the accurate value for the NME is required to study the ν mass. It, however, is extremely hard to calculate the NME by theoretical models since the NME to be studied is a tiny fraction ($\approx 10^{-4}$) of the total sum of the DBD responses and the NME is very sensitive to all kinds of nuclear correlations. Thus the calculated NMEs, including the effective axial-vector coupling (g_A^{eff}), scatter over an order of magnitude, depending on the nuclear models and the g_A^{eff} and other parameters used in the models [4–10]. Thus experimental inputs are crucial to check the theoretical models and the nuclear parameters (g_A^{eff} and others) [4,5,10–13].

Astro-νs such as the solar and supernova νs are studied via the nuclear CC interaction since the interaction rate is quite large. Then the astro-ν IBD NMEs for the ground and excited states in residual nuclei are required for the astro-ν studies. DBD nuclei and some other nuclei are used for solar-ν

real-time measurements [14–16]. The solar-ν NMEs for the excited states in ^{71}Ge are critical in views of the possible ν oscillation to the sterile ν [17]. Experimental studies for these astro-ν NMEs are needed since accurate calculations for them are difficult to obtain [4,5].

The DBD and IBD transition operators include mainly the axial-vector (isospin spin $\tau\sigma$) and the vector (isospin τ) components, and their NMEs are quenched much by the non-nucleonic $\tau\sigma$ and τ correlations and nuclear medium effects, which are hardly evaluated by theoretical models. Then g_A^{eff} and g_V^{eff} are introduced to incorporate such correlation effects that are not taken in their models. The quenching coefficients are given by g_A^{eff}/g_A and g_V^{eff}/g_V with g_A and g_V being the couplings for a free nucleon [4,5]. They are derived by comparing the absolute experimental NME with the theoretical ones.

The DBD NME includes NMEs for all intermediate states i and several multipoles J because of the medium energy (100 MeV) virtual ν. The effective couplings, reflecting the non-nucleonic nuclear medium effects, are considered to be common for them. Then it is quite realistic and effective to study absolute experimental values for some representative axial-vector dipole [Gamow-Teller (GT): 1^+] and vector dipole (V1: 1^-) NMEs to be used to check the model calculations and to get the effective couplings [5]. In fact, recent theoretical calculations show a simple linear dependence of the DBD NME on the GT component, suggesting that the GT NME represents the DBD NME [18]. The IBD NME is mainly GT NMEs for low-lying states because of the low-energy (<10 MeV) real ν. So the key point of the NME studies is to find a realistic experimental probe (way) to get exclusively the absolute GT and V1 NMEs for some representative GT and V1 states.

This Letter shows that the electric dipole ($E1$) and magnetic dipole ($M1$) γ transitions from the isobaric analog states

_____
*ejiri@rcnp.osaka-u.ac.jp

(IASs) of the initial DBD and IBD states are experimentally measured to provide the absolute values for analogous V1 and GT NMEs associated with DBDs and IBDs to check the theoretical NMEs and to provide the theories with the experimental effective axial-vector and vector couplings to help their model calculations.

Several experimental approaches to the DBD and IBD NMEs are discussed [4,5,11–13]. The charge exchange nuclear reactions (CERs) of $(^3\mathrm{He}, t)$ with sub GeV $^3\mathrm{He}$ have been used widely to estimate GT NMEs associated with DBD and IBD GT NMEs. The CER, however, includes mixed interactions of the GT($\tau\sigma$), the tensor ($[\sigma \times Y_2]_1$), and the vector (isospin:τ) interactions [5,19,20], and the cross section depends much on the nuclear distortion. Thus the CER data do not provide theories with the reliable absolute V1 and GT NMEs for individual states relevant to the DBD and IBD NMEs [4,5,11–13]. Accurate electron-capture (β^+) data are not available for DBD nuclei of current interests due to the small Q value, while β^--decay data are limited to high multipole ones, which are minor components of DBD NMEs. Beta-decay data to be used for IBD NMEs are limited to the ground state in some nuclei.

The unique features of the present IAS-EM study are as follows. (i) EM transition operators are exclusive and well-defined ones with the well-known EM couplings. Thus the observed $E1$ and $M1$ NMEs are used to get the V1 and GT NMEs and effective vector and axial-vector couplings. (ii) The absolute values for the EM NMEs are obtained experimentally by measuring the CER IAS cross sections, the IAS widths, and the CER IAS-γ cross sections. (iii) The IAS is a very sharp state, reflecting the isospin symmetry. Thus backgrounds from non-IAS excitations are small. IAS neutron decays are so reduced that the γ branch is enhanced by orders of the magnitude. (iv) The small cross section due to the small EM interaction in comparison with the large CER cross section by the strong nuclear interaction is overcome by using the IAS with the large cross section and the large γ branch and by using large acceptance detectors.

DBD, IBD and IAS-EM NMEs. The DBD rate for the light ν-mass process is expressed as [1,3,5]

$$R^{0\nu} = \ln2\, g_A^4\, G^{0\nu}[|m_\nu M^{0\nu}|]^2, \qquad (1)$$

where $G^{0\nu}$ is the phase-space factor, $g_A = 1.27$ is the axial-vector coupling for a free nucleon in units of the vector coupling of g_V, m_ν is the effective ν mass, and $M^{0\nu}$ is the NME. m_ν is replaced by the RCH term in case of the RHC process. $M^{0\nu}$ is given mainly by

$$M^{0\nu} = M^{0\nu}(\mathrm{GT}) + (g_V/g_A)^2 M^{0\nu}(V), \qquad (2)$$

where $M^{0\nu}(\mathrm{GT})$ and $M^{0\nu}(V)$ are the axial-vector (GT) and vector (V) NMEs, respectively. They are expressed in terms of the model NMEs of $M_{\mathrm{GT}}^{0\nu}$ and $M_V^{0\nu}$ as $M^{0\nu}(\mathrm{GT}) = (g_A^{\mathrm{eff}}/g_A)^2 M_{\mathrm{GT}}^{0\nu}$ and $M^{0\nu}(V) = (g_V^{\mathrm{eff}}/g_V)^2 M_V^{0\nu}$, where the effective weak couplings are introduced to incorporate such renormalization (quenching) effects of the $\tau\sigma$ and τ correlations that are not included in the model NMEs of $M_{\mathrm{GT}}^{0\nu}$ and $M_V^{0\nu}$ [5,11–13,21,22]. $M^{0\nu}$ includes also a minor tensor NME.

The NME $M^{0\nu}(\delta)$ with $\delta = \mathrm{GT}, \mathrm{V}$ is given by the sum of the NMEs $M_i^{0\nu}(\delta)$ for the intermediate states i up to around 20 MeV. The DBD proceeds as $n \to p$ and $n' \to p'$ with the ν exchange between n and n'. Then the GT and V operators are given by the double-GT (double-$\tau\sigma$) and double-V (double-τ) operators for $n \to p$ and $n' \to p'$ via the ν potential $h(\delta)$ for the medium-energy ($\approx$100 MeV) virtual ν exchanged between the two neutrons in the nucleus. Note that $h(\delta) \approx k/r_{ij}$ with r_{ij} being the distance between the two neutrons of n and n'. Then the DBD NME is given by $M^{0\nu}(\delta) = \sum_J M(\delta J)$ with $M(\delta J)$ being the J-multipole component of the NME. The single β V operator associated with the DBD V operator with the multipolarity of $J = 1$ is expressed as $f(r_i)\mathrm{Y}_1$, where $f(r_i)$ is approximately proportional to r_i. Thus it corresponds to the $E1$ γ operator $r_i\mathrm{Y}_1$. $M(\delta J)$ decreases slowly as J up to around $J \approx 6$ [5]. The real photon to be measured is the low-energy ($E \leqslant 10$ MeV) one, which is predominantly of low multipolarity. So one discusses mainly the lowest-J $M1$ and $E1$ NMEs.

The astro-ν IBD rate is expressed as [4,5]

$$R^\nu = \ln2\, g_A^2\, G^\nu f_\nu |M^\nu|^2, \qquad (3)$$

where G^ν is the phase-space factor, f_ν is the ν flux, and M^ν is the IBD NME. It is given mainly as

$$M^\nu = M^\nu(\mathrm{GT}) + (g_V/g_A)M^\nu(V), \qquad (4)$$

where $M^\nu(\mathrm{GT})$ and $M^\nu(V)$ are the axial-vector and vector NMEs for the astro-ν IBD of $\nu + n \to e + p$. They are expressed, as in DBD NMEs, in terms of the model NMEs of M_{GT}^ν and M_V^ν as $M^\nu(\mathrm{GT}) = (g_A^{\mathrm{eff}}/g_A)M_{\mathrm{GT}}^\nu$ and $M^\nu(V) = (g_V^{\mathrm{eff}}/g_V)M_V^\nu$. Actually, $M^\nu(\mathrm{GT})$ is mainly the GT($J = 1^+$) NME and $M^\nu(V)$ is the F (Fermi) ($J = 0^+$) NME for low-energy (solar) νs $\leqslant 15$ MeV, since the ν and electron momenta are much smaller than the inverse of the nuclear radius and thus the higher multipole transitions are reduced by orders of magnitudes in all nuclei. Since the Fermi decay is exclusively to IAS, one considers here mainly $M^\nu(\mathrm{GT})$ to low-lying states.

The weak NME $M^-(\alpha)$ for the α-mode β^- transition is related to the EM(γ) NME $M^{\mathrm{IA}}(\alpha')$ for the analogous α' mode IAS-γ transition as shown first in Refs. [23,24] as

$$M^-(\alpha) \approx \sqrt{2T} M^{\mathrm{IA}}(\alpha'), \qquad (5)$$

where $T = (N - Z)/2$ is the isospin of the initial (ground) state $_Z^A\mathrm{X}$ and IAS is expressed as $(\sqrt{2T})^{-1}\, T^-{}_Z^A\mathrm{X}$ with T^- being the isospin lowering operator of $n \to p$. Here A, N, and Z are the mass, neutron, and atomic numbers. The β^- NMEs $M^-(\alpha)$ with $\alpha = \mathrm{GT}, \mathrm{V1}$ are derived from the analogous IAS-γ NMEs $M^{\mathrm{IA}}(\alpha')$ with $\alpha' = M1, E1$.

DBD, IBD, IAS-EM(γ), and CER are schematically shown in Fig. 1. $M^{0\nu}$ is sensitive to the many-body nuclear and non-nuclear $\tau\sigma$ and τ correlations involved in the double-GT and double-V transitions of $(n \to p, n' \to p')$ in the DBD of $_Z^A\mathrm{X} \to _{Z+1}^A\mathrm{X} \to _{Z+2}^A\mathrm{X}$. Likewise, M^ν is sensitive to the many-body $\tau\sigma$ and τ correlations involved in the IBD of $n \to p$ in $_Z^A\mathrm{X} \to _{Z+1}^A\mathrm{X}$.

In fact, IAS-γs for the first forbidden β NMEs were studied before by using (p, γ) reactions via the strong IAS resonance
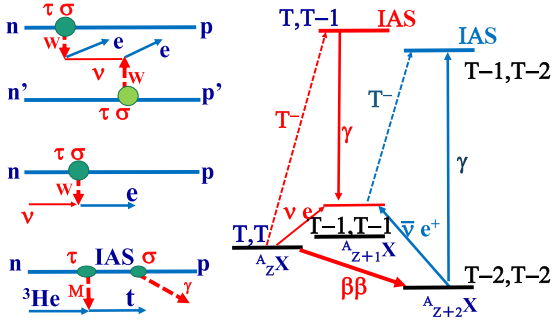
FIG. 1. Left: GT weak and IAS-$M1\gamma$ transition diagrams. Top: DBD with ν exchange between n and n'. Middle: Astro-ν IBD. Bottom: $(^3\text{He}, t)$ CER of the IAS excitation followed by EM(γ) transition. W, weak boson; M, meson; τ, isospin; σ, spin. Green circles: Nuclear $\tau\sigma$ vertexes. Green ellipsoids: Nuclear CER (τ) and $M1(\sigma)$ vertexes. In the case of $E1$ the operator σ is replaced by rY_1. Right: DBD scheme for $_Z^A\text{X} \rightarrow _{Z+2}^A\text{X}$ via the intermediate nucleus $_{Z+1}^A\text{X}$ and the γ decay from IAS (red lines) and the γ excitation to IAS (blue lines). (T, T_z) are the isospin and its z component.

with the large cross section around 10 μb [23]. However, there are no stable target nuclei for the (p, γ) reactions on DBD and astro-ν nuclei.

The IAS-γ study for axial vector and vector NMEs is found to be made by using the medium energy $(^3\text{He}, t)$ CER with $E(^3\text{He}) \approx 0.42\text{--}0.45$ GeV. Actually the CER excites strongly the IAS and GT states and is used to study GT states in DBD and astro-ν nuclei [25–36].

IAS is the isospin (τ^-) giant resonance (GR), which is strongly excited as a sharp peak in the τ^- CER. The excitation spectrum for a DBD nucleus of ^{82}Se [34] is shown as an example in Fig. 2.

The IAS differential cross section is expressed as

$$d\sigma^{\text{IA}}/d\Omega = kNJ_\tau^2 B(\text{IAS}), \qquad (6)$$

with k, N, J_τ, and $B(\text{IAS})$ being the kinematical factor including the small effect of the momentum transfer, the distortion factor, the interaction strength, and the IAS reduced width. $B(\text{IAS})$ is given by the sum rule limit of $2T_z = (N - Z)$. Thus the $d\sigma^{\text{IA}}/d\Omega$ at $0°$ for the DBD nuclei with $A = 70\text{--}160$ gets as large as 10 mb/sr.

The IAS-γ differential cross section is measured in coincidence with the IAS CER. It is given as

$$\frac{d\sigma^{\text{IA}}(\alpha')}{d\Omega} = \frac{d\sigma^{\text{IA}}}{d\Omega} \frac{\Gamma^{\text{IA}}(\alpha')}{\Gamma(T)}, \qquad (7)$$

where $\Gamma^{\text{IA}}(\alpha')/\Gamma(T)$ is the γ-branching ratio with $\Gamma^{\text{IA}}(\alpha')$ being the α' mode EM γ width and $\Gamma(T)$ being the total IAS width. Hereafter we discuss mainly IAS-$M1$ and IAS-$E1$ ($\alpha' = M1, E1$) transitions to axial-vector GT(1^+) and vector dipole V1(1^-) states.

The IAS-γ width $\Gamma^{\text{IA}}(\alpha')$ in units of eV for $\alpha' = M1, E1$ is expressed in terms of the γ ray energy $E_{\alpha'}$ in units of MeV and the γ reduced width $B^{\text{IA}}(\alpha')$ as [37,38]

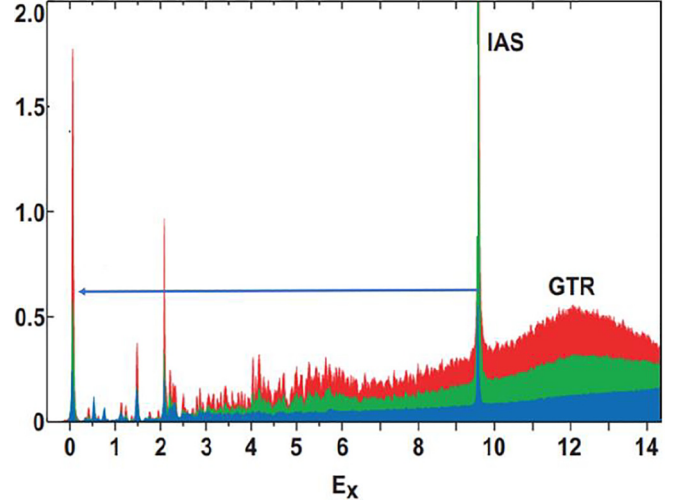$$\Gamma^{\text{IA}}(\alpha') = K_{\alpha'} E_{\alpha'}^3 B^{\text{IA}}(\alpha'), \qquad (8)$$

FIG. 2. The energy spectrum of the $(^3\text{He}, t)$ reaction on ^{82}Se [34]. The yield in units of $10^4/(\text{msr } 5\text{ keV})$ is plotted against the excitation energy in units of MeV. The IAS peak (red) at the forward angle is overscaled. See Ref. [34] for the details. The energy scale below 6 MeV is enlarged. Yields at the t emission angles of 0–0.5, 1–1.5, and 2–2.5, all in degrees, are shown by red, green, and blue, respectively. IAS and GT CERs with no angular momentum transfer are enhanced at the forward angle (red). The blue arrow is γ from IAS.

where $K_{\alpha'}$ is the kinematical factor. The reduced width is expressed by using the IAS-EM NME $M^{\text{IA}}(\alpha')$ as

$$B^{\text{IA}}(\alpha') = g_{\alpha'}^2 |M^{\text{IA}}(\alpha')|^2 S^{-1}, \qquad (9)$$

where $S = 2J_i + 1$ is the spin factor with J_i being the initial state spin and $g_{\alpha'}$ the EM coupling. The coupling is $g_{M1} = (e\hbar/2Mc)g$ with e, M, c, and g being the electron charge, the nucleon mass, the light velocity, and $M1$ g factor for the $M1$ γ, and $g_{E1} = e$ for the $E1$ γ. $M(E1)$ is in units of fm. The kinematical factor is 1.05 for $E1$ and 1.16×10^{-2} for $M1$ transitions.

The $M1$ and $E1$ γ NMEs are related to the corresponding GT and V1 β NMEs. In fact, $M1$ transition operator includes a contribution from the orbital term in addition to the spin term. In case of a spin-stretched transition of $l \pm 1/2 \leftrightarrow l \mp 1/2$, the $M1$ g factor is given effectively as $g = \sqrt{3/4\pi}(g_s/2 - g_l/2)$ with g_s and g_l being the nucleon spin and orbital g factors. Here note $g_s \gg g_l$. Actually, the major GT transitions are the spin-streched transitions of $g_{7/2} \rightarrow g_{9/2}$ and $d_{3/2} \rightarrow d_{5/2}$ for the present DBD nuclei with $A \approx 96\text{--}116$ and $A \approx 128\text{--}136$, respectively. The g_l contributions from non-spin-stretched transitions are of the order of 10% or less on the basis of the QP (quasiparticle) model. Then the orbital l contribution to the $M1$ γ NME is effectively included in the spin term by using the effective g factor and the MIγ-NME $M^{\text{IA}}(M1)$ where the $T(M1) = \sigma$ is used to get the analogous GTβ-NME with the transition operator of $T(\text{GT}) = \tau\sigma$.

In case of the $E1$ transition, the transition operator is $T(E1) = rY_1$ with r being the radius coordinate. Then $E1\gamma$-NME $M^{\text{IA}}(E1)$ with the transition operator of $T(E1)$ is used

TABLE I. $M1\gamma$ widths and the IAS γ cross sections for DBD nuclei and ^{71}Ga for the solar νs. Shown are E(IA) in units of MeV, E(GT) in units of MeV, B(GT), $B^{IA}(M1)$ in units of 10^{-2}, $\Gamma^{IA}(M1)$ in units of 10^{-2} eV, and $\sigma^{IA}(M1) = d\sigma^{IA}(M1)/d\Omega$ in units of nb (10^{-9} b)/str.

A	E(IA)	E(GT)	B(GT)	$B^{IA}(M1)$	$\Gamma^{IA}(M1)$	$\sigma^{IA}(M1)$
^{76}Ge	8.31	1.07	0.14	1.45	6.4	41
^{82}Se	9.58	0.075	0.34	3.0	30.0	150
^{96}Zr	10.9	0.69	0.16	1.25	15.3	76
^{100}Mo	11.1	0	0.35	2.7	43.4	170
^{116}Cd	12.1	0	0.14	0.88	18.0	51
^{128}Te	12.0	0	0.079	0.41	8.2	17
^{130}Te	12.7	0	0.072	0.35	8.2	17
^{136}Xe	13.4	0.59	0.23	1.03	25	45
^{150}Nd	14.4	0.11	0.13	0.54	18.0	35
^{71}Ga	8.91	0	0.085	1.2	9.8	51

TABLE II. $E1\gamma$ widths and the IAγ cross sections. Shown are E(IAS) and E(V1) in units of MeV, QP model B(V1), $B^{IA}(E1)$ in units of 10^{-2}, $\Gamma^{IA}(E1)$ in units of 10^{-2} eV, and $\sigma^{IA}(E1) = d\sigma^{IA}(E1)/d\Omega$ in units of nb (10^{-9} b)/str.

A	E(IAS)	E(V1)	B(V1)	$B^{IA}(E1)$	Γ(E1)	$\sigma^{IA}(E1)$
^{96}Zr	10.9	3	6.8	43	220	1080
^{100}Mo	11.1	3	7.5	47	260	1020
^{130}Te	12.7	3	1.0	3.8	36	75

The IAS-γ branching ratio $\Gamma^{IA}(\alpha')/\Gamma(T)$ is obtained by using the estimated $\Gamma^{IA}(\alpha')$ and the total width $\Gamma(T)$ measured experimentally. The total widths for the DBD nuclei are derived from the high-energy-resolution CERs [25,28–36] as shown in Fig. 3, together with other experimental widths [39]. They are given by

$$\Gamma(T) \approx 3.5 T_z \text{ keV}, \quad T_z = (N - Z)/2. \quad (10)$$

The IAS width is indeed very small in comparison with a typical neutron width of the order of MeV.

Then the IAS-$M1\gamma$ and IAS-$E1\gamma$ cross sections at $0°$ are estimated by using the measured IAS cross section at $0°$, the experimental $\Gamma(T)$ and the estimated $B^{IA}(M1)$ and $B^{IA}(E1)$ values as given in Tables I and II. The IAS-$M1\gamma$ and IAS-$E1\gamma$ cross sections are of the orders of 10–100 nb and 100–1000 nb/sr, respectively. The estimated IAS-γ cross sections for the $M1$ and $E1$ transitions are about 10^{-6}–10^{-4} of the IAS ones of 10 mb, reflecting the $M1$ and $E1$ γ branching ratios to the total IAS width. The $E1$ cross sections are larger by one to two orders of magnitude than the $M1$ cross sections because of the larger kinematical factor in Eq. (8). The very small $d^{IA}\sigma(E1)/d\Omega$ for ^{130}Te is due to the small U (vacancy coefficient). The cross sections are shown in Fig. 4.

IAS-γ event rates under typical experimental conditions are estimated to show the feasibility of the experimental studies. Using a target of 40 mg/cm^2, a ^{3}He beam of 20 npA, and a spectrometer of a solid angle of 3.2 msr, the IAS-γ event

to get the analogous V1β-NME with the transition operator of $T(V1) = \tau r Y_1$.

Actual procedures to get the β NMEs associated with the DBD and IBD NMEs are (i) excite the IAS by the $(^3$He$, t)$ reaction on ^A_ZX (see Fig. 1) and measure the IAS differential cross section $d\sigma^{IA}/d\Omega$ and the IAS total width $\Gamma(T)$, (ii) obtain the IAS-γ differential cross section $d\sigma^{IA}(\alpha')/d\Omega$ with $\alpha' = M1, E1$ for low-lying 1^+ and 1^- states in $^A_{Z+1}$X by measuring the γ-rays in coincidence with the IAS CER, (iii) obtain the reduced γ widths $\Gamma^{IA}(\alpha')$ by using the measured IAS and IAS-γ differential cross sections and the measured total width $\Gamma(T)$ in Eq. (7), (iv) obtain the reduced γ width $B^{IA}(\alpha')$ from the measured γ width $\Gamma^{IA}(\alpha')$ in Eq. (8) and the γ NME $M^{IA}(\alpha')$ by using the $B^{IA}(\alpha')$ in Eq. (9), and (v) get the β^- NMEs $M^-(\alpha)$ with $\alpha = $ GT,V1 from the $M^{IA}(\alpha')$ with $\alpha' = M1, E1$ in Eq. (5).

IAS-γ cross sections. The IAS-γ cross sections for realistic cases of the GT and V1 transitions and the experimental counting rates are estimated to show the feasibility of the experiment.

The IAS-$M1$ widths Γ_{M1} for GT states in DBD and IBD nuclei are estimated by using the NMEs M(GT) for low-lying states in the DBD and astro-ν nuclei. One uses the GT states with relatively large B(GT) of the order of 10^{-1}, which are considered to be the spin-stretched GT transitions. The reduced widths $B^{IA}(M1)$ are estimated by assuming the CER B(GT) derived without considering the tensor term interference [25,28–36]. The IAS-$M1$ γ widths $\Gamma^{IA}(M1)$ are estimated as shown in Table I.

The IAS-$E1$ γ widths $\Gamma^{IA}(E1)$ for V1 1^- states in DBD nuclei are estimated by using the QP model V1 NMEs $M(V1)$ since the V1 β reduced widths in DBD nuclei are not known experimentally. The V1 NMEs for QP states in medium heavy nuclei have been shown to be approximately given by the QP model with experimental effective coupling of $g_{E1}^{\text{eff}}/g_{E1} \approx$ 0.2–0.25 [23,24,38]. So the V1 NMEs for the typical V1 transitions of $n(1h_{11/2}) \to p(1g_{9/2})$ in 3 DBD nuclei are estimated by using the QP NMEs with the effective coupling of $g_{E1}^{\text{eff}}/g_{E1} = 0.225$. They are shown in Table II.
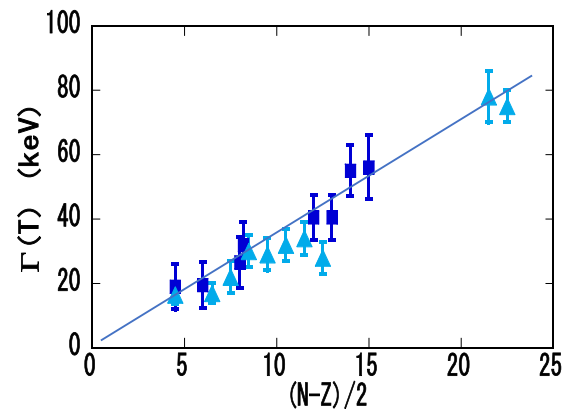

FIG. 3. Experimental IAS widths as a function of the isospin $T_z = (N - Z)/2$. Blue squares for IASs in DBD nuclei derived in the present work. Light blue triangles from Ref. [39].
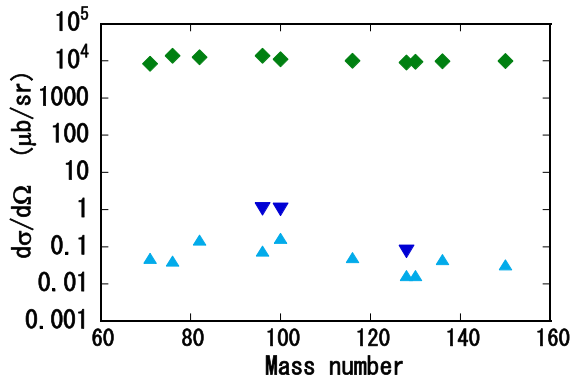
FIG. 4. Differential cross sections at $0°$ for DBD and astro-ν nuclei. Green diamonds: IAS excitations. Blue inverse triangles: IAS-$E1\gamma$s to 1^- states. Light blue triangles: IAS-$M1\gamma$s to 1^+ states.

rate per day is

$$R_\gamma = 8A^{-1}10^2(d\sigma^{IA}(\alpha')/d\Omega)\epsilon_\gamma, \qquad (11)$$

where A, $d\sigma^{IA}(\alpha')/d\Omega$, and ϵ_γ are the target mass number, the differential cross section with $\alpha' = M1, E1$ in units of nb/sr, and the γ detection efficiency. Recent developments of γ detectors have made it possible to measure γ rays with the efficiency around 5–10% [40–42]. Then one gets $Y \approx 50$ per day in case of $\epsilon \approx 6\%$ and $d\sigma^{IA}(\alpha')/d\Omega \approx 100$ nb at the solid angle window. Then the IAS-γ experiments to get accurate ($\pm 10\%$ or so) NMEs are quite feasible.

Concluding remarks. The IAS-EM(γ) study opens a new experimental way to access the DBD and IBD NMEs, which are crucial for neutrino studies in complex nuclei. It provides absolute values for $M1-E1$ NMEs with well-defined EM operators and the EM couplings. They are used to obtain the corresponding weak GT-V1 NMEs and the effective weak couplings, which are associated with DBD and IBD NMEs. They are free from uncertainties due to the other interfering NMEs due to other interactions [43] and the distortion potential as in the CERs used so far. The IAS-γ coincidence leads to background-free measurements. The event rates estimated

for GT and V1 states in DBD and IBD nuclei indicate the feasibility of the experiments with available detectors.

Then DBD and IBD nuclear models and their nuclear parameters (g_A^{eff}, g_V^{eff}, g_{pp}, etc.) are well checked by comparing the calculated GT and V1 (IAS-$M1$ and IAS-$E1$) NMEs by using the DBD and IBD models with the experimental GT and V1 (IAS-$M1$ and IAS-$E1$) NMEs derived from the IAS-EMγ experiments. The experimental g_{M1}^{eff} and g_{E1}^{eff} help evaluate the g_A^{eff} and g_V^{eff} used for DBD and IBD models since calculations for them are hard.

The experimental GT and V1 NMEs studied by the IAS-EM(γ), together with the experimental β and $2\nu\beta\beta$ NMEs and the experimental GT and SD (spin-dipole) GRs studied by CERs [13], are very powerful in pinning down the DBD and astro-ν NMEs.

EM(γ) excitations to IAS are used for studying the n$'$-p$'$ $M'(\alpha)$ (right leg) NMEs associated with DBDs and astro-$\bar{\nu}$s as shown in Fig. 1 (blue lines) [44]. The measured EM NMEs for low-lying states are used to check the DBD and IBD models and to provide them with the effective g_A^{eff}/g_A and g_V^{eff}/g_V to be used. Then the product of $M \times M'$ gives the product of the couplings relevant to the DBD NME. Actually the Fermi surface quasiparticle model with experimental inputs of the NMEs of $M(GT)$ and $M'(GT)$ reproduces the observed $2\nu\beta\beta$ NMEs [45].

Studies of EM(γ) decays from GT-GR excited by CER provide the GT NME and the g_A^{eff} for the GT GR. Comparison of GT NMEs derived from the IAS-$M1$ (γ) studies and the GT NMEs derived from CERs may show the possible tensor interference effect.

The present low-energy (<10 MeV) IAS-EM(γ) probe emphasizes realistic measurements of the accurate absolute values for the GT(1^+) and V1(1^-) NMEs, which are key ingredients for the DBD and IBD NMEs and their effective axial-vector and vector couplings. Note that medium-energy ($E \approx 100$ MeV) ν, μ^+, and γ probes might excite in principle very many states in wide ranges of the multipoles (J) and excitation energies (E_i) as the DBD virtual ν, but the cross sections would be formidably small and selections of states with specific J and E_i would not be experimentally possible. Double CERs and double γs are interesting challenges in the future [18,46,47].

[1] H. Ejiri, J. Phys. Soc. Jpn. **74**, 2101 (2005).
[2] F. T. Avignone, III, S. R. Elliott, and J. Engel, Rev. Mod. Phys. **80**, 481 (2008).
[3] J. Vergados, H. Ejiri, and F. Šimkovic, Rep. Prog. Phys. **75**, 106301 (2012).
[4] H. Ejiri, Phys. Rep. **338**, 265 (2000).
[5] H. Ejiri, J. Suhonen, and K. Zuber, Phys. Rep. **797**, 1 (2019).
[6] A. Faessler and F. Simkovic, J. Phys. G: Nucl. Part. Phys. **24**, 2139 (1998).
[7] J. Suhonen and O. Civitarese, J. Phys. G: Nucl. Part. Phys. **39**, 085105 (2012).
[8] J. Barea, J. Kotila, and F. Iachello, Phys. Rev. C **87**, 014315 (2013).
[9] J. Engel and J. Menéndez, Rep. Prog. Phys. **80**, 046301 (2017).

[10] L. Jokiniemi, H. Ejiri, D. Frekers, and J. Suhonen, Phys. Rev. C **98**, 024608 (2018).
[11] H. Ejiri, Universe **6**, 225 (2020).
[12] H. Ejiri, Front. Phys. **9**, 650421 (2021).
[13] H. Ejiri, L. Jokiniemi, and J. Suhonen, Phys. Rev. C **105**, L022501 (2022).
[14] H. Ejiri, J. Engel, R. Hazama, P. Krastev, N. Kudomi, and R. G. H. Robertson, Phys. Rev. Lett. **85**, 2917 (2000).
[15] K. Zuber, Phys. Lett. B **571**, 148 (2003).
[16] R. S. Raghavan, Phys. Rev. Lett. **37**, 259 (1976).
[17] V. V. Barinov *et al.*, Phys. Rev. Lett. **128**, 232501 (2022).
[18] N. Shimizu, J. Menendez, and K. Yako, Phys. Rev. Lett. **120**, 142502 (2018).
[19] W. Haxton, Phys. Lett. B **431**, 110 (1998).

[20] J. Kostensalo *et al.*, Phys. Lett. B **795**, 542 (2019).

[21] J. Suhonen, Phys. Rev. C **96**, 055501 (2017).

[22] H. Ejiri, Front. Phys. **7**, 30 (2019).

[23] H. Ejiri, P. Richard, S. Ferguson, R. Heffner, and D. Perry, Phys. Rev. Lett. **21**, 373 (1968).

[24] H. Ejiri and J. I. Fujita, Phys. Rep. **38**, 85 (1978).

[25] H. Akimune *et al.*, Phys. Lett. B **394**, 23 (1997); **665**, 424 (2008).

[26] H. Ejiri *et al.*, Phys. Lett. B **433**, 257 (1998).

[27] D. Frekers *et al.*, Phys. Lett. B **706**, 134 (2011).

[28] J. H. Thies *et al.*, Phys. Rev. C **86**, 014304 (2012).

[29] J. H. Thies *et al.*, Phys. Rev. C **86**, 054323 (2012).

[30] P. Puppe, D. Frekers, T. Adachi, H. Akimune, N. Aoi, B. Bilgier, H. Ejiri, H. Fujita, Y. Fujita, M. Fujiwara, E. Ganioğlu, M. N. Harakeh, K. Hatanaka, M. Holl, H. C. Kozer, J. Lee, A. Lennarz, H. Matsubara, K. Miki, S. E. A. Orrigo, T. Suzuki, A. Tamii, and J. H. Thies, Phys. Rev. C **84**, 051305(R) (2011).

[31] C. J. Guess *et al.*, Phys. Rev. C **83**, 064318 (2011).

[32] J. H. Thies *et al.*, Phys. Rev. C **86**, 044309 (2012).

[33] P. Puppe *et al.*, Phys. Rev. C **86**, 044603 (2012).

[34] D. Frekers *et al.*, Phys. Rev. C **94**, 014614 (2016).

[35] H. Ejiri and D. Frekers, J. Phys. G: Nucl. Part. Phys. **43**, 11LT01 (2016).

[36] D. Frekers, P. Puppe, J. H. Thies, and H. Ejiri, Nucl. Phys. A **916**, 219 (2013).

[37] A. Bohr and B. Mottelson, *Nuclear Structure II* (W. A. Benjamin, Amsterdam, 1975).

[38] H. Ejiri and M. A. deVoigt, *Electron and Gamma-ray Spectroscopy in Nuclear Physics* (Oxford University Press, Oxford, 1988).

[39] H. L. Harney, A. Richter, and A. Weidenmüller, Rev. Mod. Phys. **58**, 607 (1986).

[40] A. Giaz *et al.*, Nucl. Instrum. Methods A **729**, 910 (2013).

[41] N. Kobayashi *et al.*, Eur. Phys. J. A **55**, 231 (2019).

[42] A. Tamii and N. Kobayashi, Technical Report, RCNP (2022).

[43] M. A. Franey and W. G. Love, Phys. Rev. C **31**, 488 (1985).

[44] H. Ejiri, A. Titov, M. Bosewell, and A. Yang, Phys. Rev. C **88**, 054610 (2013).

[45] H. Ejiri, J. Phys. G: Nucl. Part. Phys. **44**, 115201 (2017).

[46] F. Cappuzzello *et al.*, Prog. Part. Nucl. Phys. **128**, 103999 (2023).

[47] B. Romeo, J. Menéndez, and C. Pena, Phys. Lett. B **827**, 136965 (2022).